Catalysis Science & Technology

Accepted Manuscript

ROYAL SOCIETY OF CHEMISTRY

www.rsc.org/catalysis

Journal Name

ARTICLE

Solubility Product Difference-Guided Synthesis of Co_3O_4-CeO_2 Core-Shell Catalysts for CO Oxidation

Received 00th January 20xx,
Accepted 00th January 20xx

DOI: 10.1039/x0xx00000x

www.rsc.org/

Guozhu Chen,[a,*] Qihui Xu,[a] Yong Wang,[a] Guolong Song,[a] Cuncheng Li,[a] Wei Zhao,[b] Weiliu Fan[c]

It is still an important issue of developing a facile, environmental way to synthesize bimetal oxide materials. In this paper, Co_3O_4-CeO_2 core-shell catalysts were prepared by an interfacial reaction, where $Co(CO_3)_{0.35}Cl_{0.2}(OH)_{1.1}$ nanorods were dispersed in Ce^{3+} aqueous solution for 2 days, followed by a calcination step. The samples were characterized by X-ray diffraction (XRD), transmission electron microscopy (TEM), and X-ray photoelectron spectroscopy (XPS). Based on the characterization and comparative experimental results, we proposed that the OH^- ions slowly dissociated from $Co(CO_3)_{0.35}Cl_{0.2}(OH)_{1.1}$ precursor combine with Ce^{3+} to develop into $Ce(OH)_3$ nanoparticles because of its smaller solubility product constant than that of Co precursor or $Co(OH)_2$. Neither additional precipitation agent nor stabilizing molecules were employed during the whole preparation. Raman spectroscopy and H_2-Temperature program reduction (H_2-TPR) analysis revealed that there is a synergistic effect between Co_3O_4 and CeO_2 in the as-prepared Co_3O_4-CeO_2 core-shell catalysts, which is responsible for their enhanced catalytic activity toward CO oxidation in comparison to pure Co_3O_4 and CeO_2.

1. Introduction

It is well known that ceria (CeO_2) is a key component in the formulation of catalysts owing to its excellent redox property and high oxygen storage capacity, thus, has attracted tremendous interest in fundamental studies and practical applications.[1-14] Over the last decade, the synthesis of CeO_2-based bimetal oxide catalysts and the optimization of their size, morphology, and composition were extensively studied because some bimetal oxides exhibit remarkable properties distinctly different from their monometallic counterparts, known as the synergistic effect in catalysis due to the interaction between two oxides.[15-26] During the catalytic reactions, the interfacial contact between CeO_2 and secondary metal oxide is proposed to be active site, which is of great importance in determining their catalytic performance. Therefore, from a structural viewpoint, a considerable contact within components is highly expected in a good catalyst, which can enable an efficient diffusion of reactants into the active sites. Until now, co-precipitation,[27] impregnation[28] and sol-gel[29] approaches are widely used to prepare CeO_2-based bimetal oxides. Although the components mix well even at the atomic level, the exposure of the active sites to reactants is suppressed for the catalysts prepared using the former two routes, except in the case of the utilization of specific templates (*e.g.* mesoporous templates).[28] Since the hydrolysis and condensation rates of the precursors differ considerably, phase separation is ineluctable during the sol-gel process, thus leading to the decrease in contact within components.[29]

To address the issues above, the fabrication of bimetal oxides with core-shell structures by depositing the secondary shell onto the pre-synthesized core surface seems feasible, because the sufficient contact between core and shell is guaranteed in this kind of structure.[20,21,30,31] However, the conventional layer-by-layer technique is a multistep process that requires precise control in surface modification and shell deposition. Specifically, to avoid homogeneous nucleation of the shell component, it is necessary to perform a surface modification to the core with the assistance of organic species (*e.g.* polymers or surfactants). Because the heterogeneously catalytic reaction occurs on the catalyst surface, these organic species need to be removed so as to fully expose the surface active sites. Unfortunately, a complete removal of these organic species is still challenging, and hence resulting in the deactivation of the catalyst. Moreover, the organic compounds and precipitation agents for the shell deposition always need to be carefully chosen. Obviously, this method is not economically feasible for a mass production of catalysts and is not preferred in industrial fields. Therefore, it is of highly interest to develop a surface modification-free, and easily scale-up approach to synthesize bimetal oxide catalysts with core-shell structure.

Solid-liquid interfacial reaction, proceeded by a sacrificial solid template reacting with one designated solution, has been identified as an effective method to synthesize core-shell structured materials. In this method, the surface modification-free manipulation can be realized as the formation of new shells is merely driven by the chemical reactions between templates and ions in solution. For example, a simple redox reaction in Ce^{4+} ion solution with the presence of Cu_2O as the sacrificial template leads to the formation of Cu_2O-CeO_2 core-shell bimetal oxides.[20] Recently, we also prepared CeO_2-MnO_2 bimetal oxides by treating $Ce(OH)CO_3$ templates with $KMnO_4$ aqueous solution, where MnO_4^- is reduced to MnO_2 and the Ce^{3+} in $Ce(OH)CO_3$ is simultaneously oxidized to form CeO_2.[32] In addition to the redox interfacial reaction, ion exchange is a well-

[a]School of Chemistry and Chemical Engineering, University of Jinan No.336 Nanxinzhuang west road, Jinan (P. R. China) Tel: (86)-531-82769181; E-mail: chm_chengz@ujn.edu.cn
[b]Shandong Institute and Laboratory of Geological Sciences
[c]School of Chemistry and Chemical Engineering, Shandong University

known way to synthesize core-shell nanomaterials. For example, Cu_2O-Cu_2S core-shell structure can be achieved upon the addition of Cu_2O templates into Na_2S solution due to the small solubility product constant of Cu_2S ($K_{sp}=10^{-48}$).[33] So far, the ion exchange procedure is restricted to chalcogenide based core-shell nanomaterials,[34] in contrast, the synthesis of bimetal oxide with core-shell structures via an ion exchange method has not been extensively studied yet.

In this paper, we choose Co_3O_4-CeO_2 nanostructure as an example to demonstrate the interfacial process capable of generating core-shell bimetal oxides. Co_3O_4-CeO_2 bimetal oxide is an interesting catalyst that was studied in CO, hydrocarbon and diesel oxidation reactions.[24,25,29,30] Herein, Co_3O_4-CeO_2 core-shell structured nanorods were successfully fabricated by easily reacting the $Co(CO_3)_{0.35}Cl_{0.2}(OH)_{1.1}$ nanorods with Ce^{3+} aqueous solution, followed by calcination. Compared to the traditional synthetic process, neither additional precipitation agent nor stabilizing molecules are involved during the whole preparation. The solubility product difference between $Ce(OH)_3$ and the employed Co precursor plays the key role for the formation of the CeO_2 shell.

2. Experimental

2.1 Materials

Cobalt chloride hexahydrate ($CoCl_2{\cdot}6H_2O$) were purchased from Aladdin Industrial Corporation, urea (H_2NCONH_2), cerium(III) nitrate hexahydrate ($Ce(NO_3)_3{\cdot}6H_2O$), ammonium cerium(IV) nitrate ($(NH_4)_2Ce(NO_3)_6$) and ethanol were purchased from Sinopharm Chemical Reagent Co. Ltd. They were of analytical grade and were used without further purification.

2.2 Synthesis of the $Co(CO_3)_{0.35}Cl_{0.2}(OH)_{1.1}$ precursor

$Co(CO_3)_{0.35}Cl_{0.2}(OH)_{1.1}$ can be easily prepared by mixing $CoCl_2$ and urea.[24] In a typical synthesis, 1.1897 g (5 mmol) of $CoCl_2{\cdot}6H_2O$ was first dissolved in 40 mL of deionized water under vigorous magnetic stirring and 300.3 mg (5 mmol) of urea was then added into the water solution. The obtained claret-red solution was transferred into a Teflon-lined steel autoclave and heated at 100 °C for 12 h in an electric oven. After the autoclave was cooled to room temperature, pink products were collected and washed with deionized water and ethanol three times and dried overnight at 80 °C.

2.3 Synthesis of the Co_3O_4-CeO_2, pure Co_3O_4 and CeO_2

Different amounts of $Ce(NO_3)_3$ were dissolved in 30 mL of deionized water under stirring. Then the as-prepared $Co(CO_3)_{0.35}Cl_{0.2}(OH)_{1.1}$ was added into the above clear solutions and kept still for 2 days. Finally, the samples were thoroughly washed with ultrapure water, dried, followed by a calcination at 550 °C for 4 h.

Pure Co_3O_4 was synthesized from direct thermal decomposition of $Co(CO_3)_{0.35}Cl_{0.2}(OH)_{1.1}$ at 550 °C for 4 h. In the case of pure CeO_2, it was prepared by mixing $Ce(NO_3)_3$ and NaOH solution. Then the product was washed with deionized water, dried and calcined at 550 °C for 4 h.

2.4 Characterization

The phases and purity of the prepared samples were examined by X-ray powder diffraction (XRD) performed on a Rigaku D/Max-γA rotating anode X-ray diffractometer with Cu Kα radiation (λ = 1.54178 Å). N_2 adsorption–desorption isotherms were measured at 77 K on a Micromeritics TriStar II 3020 surface area & pore size analyzer. Before measurement, the samples were outgassed in a vacuum at 300 °C for 4 h. The Brunauer-Emmett-Teller (BET) method was used to calculate the surface areas of the samples. The morphology and structure of samples were observed by transmission electron microscopy (TEM, JEM 2100) equipped with an energy dispersive X-ray spectrometer (EDS). X-ray photoelectron spectrometer (XPS) spectra were recorded by a PHI 5300 X-ray photoelectron spectrometer with Al Kα radiation. Micro-Raman measurement was conducted with an LabRAM HR Evolution High Resolution Raman Spectrometer. H_2-Temperature-programmed reduction (H_2-TPR) experiment was performed with a thermal conductivity detector on 50 mg sample using a gas mixture composed of 95% (molar) argon and 5% (molar) hydrogen at a flow rate of 30 mL min^{-1}. The temperature ramping rate was set to be 10 K min^{-1}. The CeO_2 contents in Co_3O_4-CeO_2 samples were determined using inductively coupled plasma mass spectrometer (ICP-MS, Thermo Scientific XSeries-2).

2.5 Catalyst Test

Catalytic activity was tested using a continuous flow fixed-bed micro-reactor at atmospheric pressure. In a typical experiment, the system was first purged with high purity N_2 gas and then a gas mixture (1% CO, 10% O_2, 89% N_2) passed through the reactor at a flow rate of 50 mL/min, corresponding to a space velocity of 60 000 $mL{\cdot}h^{-1}{\cdot}g^{-1}$ of catalyst. Composition of the gas exiting from the reactor was analyzed with an online infrared gas analyzer (Gasboard-3100, China Wuhan Cubic Co.), which can simultaneously detect CO, CO_2 and O_2.

3. Results and discussion

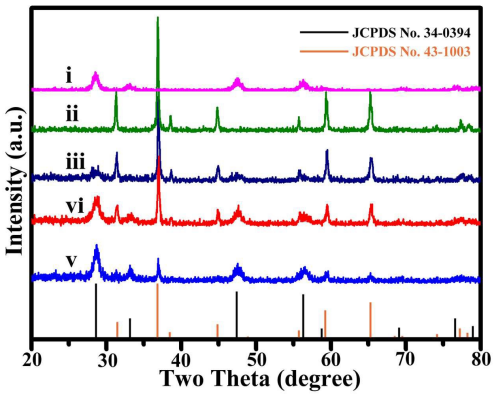

Fig. 1 XRD patterns of pure CeO_2 (i), Co_3O_4 (ii), and Co_3O_4-CeO_2 bimetal oxide catalysts with different CeO_2 compositions: 18.5 wt% (iii), 41.7 wt% (iv) and 63.4 wt% (v).

After interfacial reaction and heat-treatment at 550 °C, there are two sets of diffraction peaks, one set is corresponding to fluorite-phase CeO_2 (JCPDS no.34-0394), and the other one is indexed to spinel-phase Co_3O_4 (JCPDS no.43-1003) (Fig. 1), suggesting that Co_3O_4-CeO_2 composite can be successfully synthesized through an interfacial reaction of $Co(CO_3)_{0.35}Cl_{0.2}(OH)_{1.1}$ precursor and Ce^{3+} followed by a thermal-treatment. Moreover, the relative intensity of CeO_2 diffractions is gradually enhanced as the increase of the Ce/Co

mole ratio, suggesting that the CeO_2 content is tunable by simply varying the Ce^{3+} concentration during the interfacial reaction.

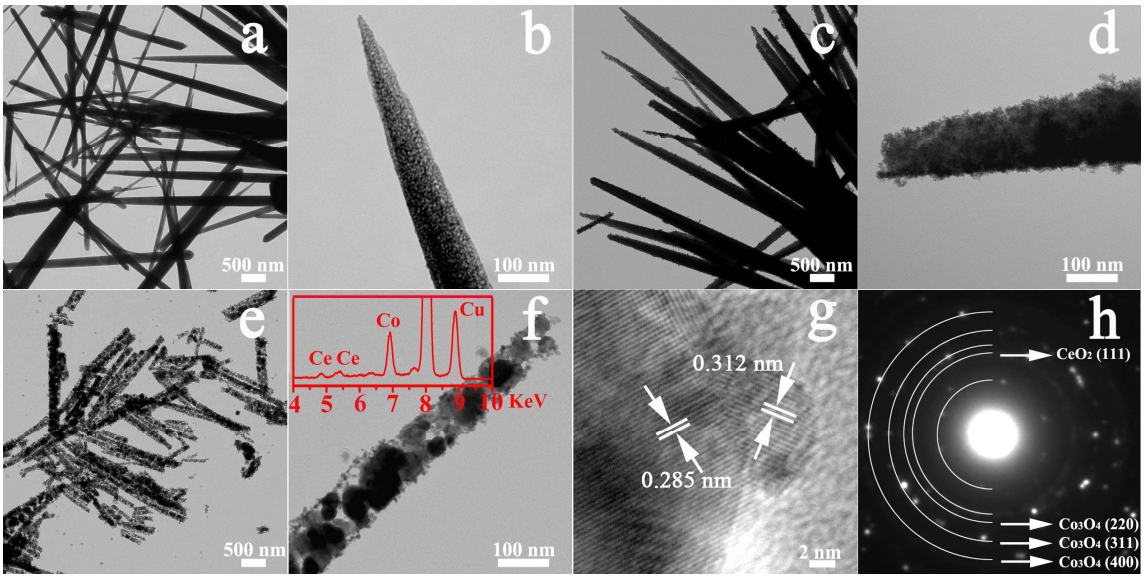

Fig. 2 TEM images of the $Co(CO_3)_{0.35}Cl_{0.2}(OH)_{1.1}$ precursor (a, b), the sample obtained by reacting Co precursor with Ce^{3+} ions before (c, d) and after calcination (e-g), and SAED pattern (h) of the Co_3O_4-CeO_2-18.5 wt% bimetal oxide catalyst. Inset in (f) is the EDS result detected from the rod in (f).

The morphologies of the $Co(CO_3)_{0.35}Cl_{0.2}(OH)_{1.1}$ precursor and the Co_3O_4-CeO_2 bimetal oxide are characterized by TEM. As shown in Fig. 2a, the Co precursor is characteristic of one-dimensional (1D) rod(or needle) structure. The rod with a smooth surface is of several micrometers in length and average 80 nm in width (Fig. 2b). After dispersing Co precursor into the $Ce(NO_3)_3$ solution, there are some dispersed nanoparticles (NPs) depositing on the Co precursor surface, as shown in Fig. 2c,d. Upon calcination, the one-dimensional structure is still maintained although the length of the rods becomes short. Higher magnification TEM image of the rod demonstrates that unlike the structure prior to the interfacial reaction, at this stage the rod turns less compact and is constructed by interconnected NPs surrounded by a NP-string-like thin shell (Fig. 2e,f). The co-existence of Ce and Co in the as-prepared sample is also supported by Energy Dispersive Spectroscopy (EDS) measurement (inset of Fig.2f). Fig. 2g shows the HR-TEM image of the interface of the core-shell structure, constituted with interfused NPs. The lattice spacings of 0.312 nm and 0.285 nm correspond well to the (111) crystal plane of the fluorite-structured CeO_2, and the (220) plane of the spinel-phase of Co_3O_4, respectively. These results regarding crystalline structure are consistent with that obtained from selected area electron diffraction (SAED) pattern shown in Fig. 2h, where two sets of diffraction rings belonging to the fluorite-phase CeO_2, and spinel-phase Co_3O_4 can be recognized.

The chemical bonding states of the core-shell structure are further investigated by XPS analysis. Fig 3 shows the XPS spectra of the typical Co_3O_4-CeO_2 sample with CeO_2 content of ~18.5 %. The coexistence of Co and Ce can be clearly observed from the wide spectrum (Fig. 3a). Fig 3b presents the high resolution XPS spectrum of Ce 3d, where the peaks can be assigned to four pairs of spin-orbit doublets: the doublets (v ~882.05 eV, u ~900.45 eV), ($u^{//}$ ~906.97 eV, $v^{//}$ ~888.26 eV), and ($u^{///}$ ~916.34 eV, $v^{///}$ ~897.94 eV) are characteristic of Ce^{4+} state, whereas the doublet ($u^{/}$ ~902.19 eV and $v^{/}$ ~884.34 eV) is indicative of Ce^{3+} state, indicating the existence of Ce^{3+} species in the as-prepared Co_3O_4-CeO_2 sample. In the case of O 1s XPS spectrum (Fig. 3c), two identical peaks are clearly displayed, indicating the presence of multi oxygen species. The peak at the lower binding energy side (O_α: 529-530 eV) is ascribed to lattice oxygen and the shoulder peak at higher banding

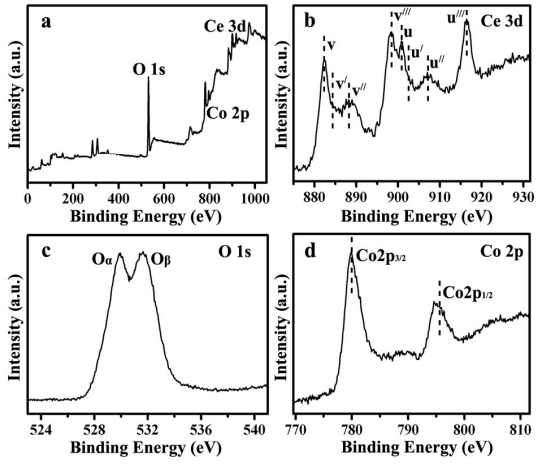

Fig. 3 XPS wide spectrum (a), high resolution XPS spectra of Ce 3d (b), O 1s (c) and Co 2p(d) spectra of the Co_3O_4-CeO_2-18.5 wt% bimetal oxide catalyst.

energy side (O_β: 531-532.8 eV) can be assigned to defective or adsorptive oxygen species. The Co 2p XPS spectrum in Fig. 3d

shows two major peaks at 795.5 and 780.4 eV which are corresponding to Co $2p_{1/2}$ and Co $2p_{3/2}$ spin-orbit signals, respectively. These results demonstrate that the surface of the Co_3O_4-CeO_2 core-shell sample is not fully covered with CeO_2 within the detection range of XPS.

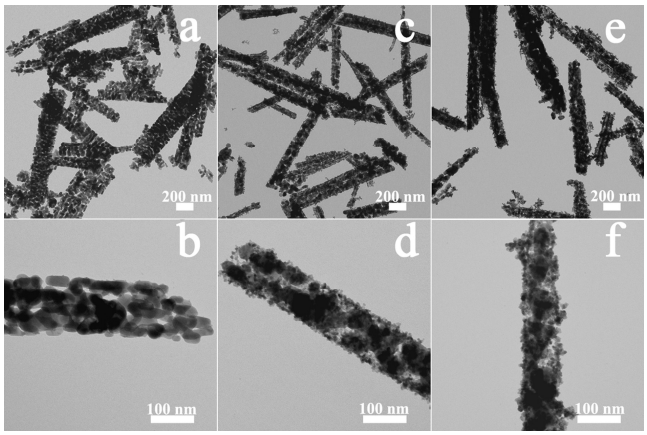

Fig. 4 TEM images of the pure Co_3O_4 (a, b) derived from the thermal decomposition of $Co(CO_3)_{0.35}Cl_{0.2}(OH)_{1.1}$ precursor, Co_3O_4-CeO_2-41.7 wt%(c, d) and Co_3O_4-CeO_2-63.4 wt% (e, f).

By simply changing the Ce^{3+} concentration, a series of Co_3O_4-CeO_2 bimetal oxides with different surface coverage of CeO_2 are obtained. Fig.4a, b shows the pure Co_3O_4 nanorods derived from the thermal decomposition of $Co(CO_3)_{0.35}Cl_{0.2}(OH)_{1.1}$, which leads to the volume shrinkage and generates subsequent porosity structure throughout the rod (Fig. 4b). After interfacial reaction and heat-treatment, compared with that shown in Fig. 2f, more dense CeO_2 NPs are formed around the rod surface as the concentration of $Ce(NO_3)_3$ increases (Fig. 4c-f). Specifically, a considerable surface coverage is reached for the sample with CeO_2 content of ~ 63.4 wt % (Co_3O_4-CeO_2-63.4 wt %) as shown in Fig. 4e and f. In the Co_3O_4-CeO_2-18.5 wt% and 41.7 wt% samples, the surface coverage by CeO_2 is less pronounced, where the shell is constructed by discontinuous CeO_2 NPs. In principle, this kind of structure enables more interfaces between Co_3O_4 and CeO_2 to expose.

When the $Co(CO_3)_{0.35}Cl_{0.2}(OH)_{1.1}$ precursor is added into $Ce(NO_3)_3$ aqueous solution, Co^{2+}, CO_3^{2-}, Cl^- and OH^- ions are slowly dissociated simultaneously, and the released OH^- ions prefer to combine with Ce^{3+} to form $Ce(OH)_3$ due to the smaller solubility product constant of $Ce(OH)_3$ ($K_{sp}=1.6\times10^{-20}$). The newly produced $Ce(OH)_3$ nucleates *in situ* and grows on the surface of the $Co(CO_3)_{0.35}Cl_{0.2}(OH)_{1.1}$ rods. Upon calcination, $Ce(OH)_3$ easily transferred into CeO_2. Meanwhile, the residual $Co(CO_3)_{0.35}Cl_{0.2}(OH)_{1.1}$ precursor is converted into Co_3O_4 eventually to form Co_3O_4-CeO_2 bimetal oxide.

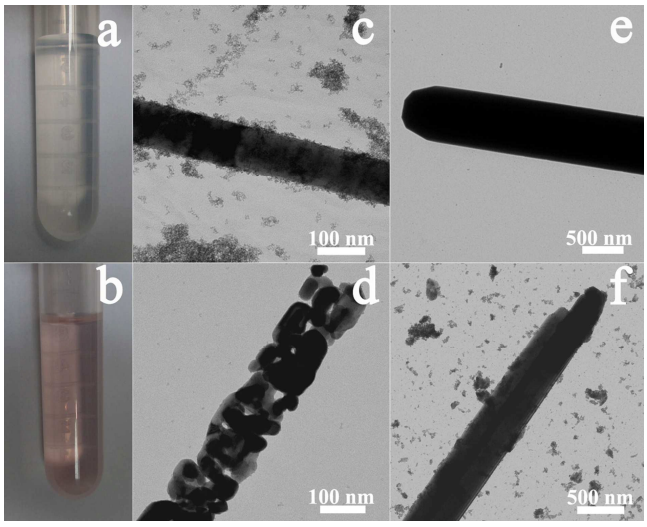

Fig. 5 Photographs of the supernatant obtained from Co_3O_4 rods (a) and Co precursor (b) dispersing into Ce^{3+} aqueous solution; TEM images of Co precursor (c) and pure Co_3O_4 (d) dispersed in Ce^{4+} aqueous solution, and TEM images of $Ce(OH)CO_3$ precursor dispersed in Ce^{3+} (e) and Ce^{4+} (f) aqueous solution.

To further understand the transformation mechanism during the interfacial reaction, Co_3O_4 rods derived from $Co(CO_3)_{0.35}Cl_{0.2}(OH)_{1.1}$ are used as a Co precursor. Obviously, the supernatant still keeps colorless when Co_3O_4 rods are dispersed in Ce^{3+} aqueous solution even for more than 2 days (Fig. 5a). By stark contrast, light pink, characteristic color of Co^{2+} ions, appears when $Co(CO_3)_{0.35}Cl_{0.2}(OH)_{1.1}$ is dispersed in Ce^{3+} aqueous solution for 2 days, as illustrated in Fig. 5b. In another case, $(NH_4)_2Ce(NO_3)_6$ instead of $Ce(NO_3)_3$ aqueous solution is mixed with $Co(CO_3)_{0.35}Cl_{0.2}(OH)_{1.1}$ precursor, TEM result verifies that in addition to NPs depositing on the rod surface, a lot of "free" particles are individually dispersed in solution (Fig. 5c), possibly due to the smaller solubility product constant of $Ce(OH)_4$ ($K_{sp}=2\times10^{-48}$) than that of $Ce(OH)_3$ ($K_{sp}=1.6\times10^{-20}$). A crossover experiment was performed by dispersing Co_3O_4 rods in $(NH_4)_2Ce(NO_3)_6$ aqueous solution for 2 days, TEM analysis confirms that no small particles formed on the Co_3O_4 rod surface (Fig. 5d). According to above phenomena, one can rule out the possibility that the formation of CeO_2 is due to the hydrolysis of Ce^{4+}. Similarly, when $Ce(OH)CO_3$ nanorods instead of $Co(CO_3)_{0.35}Cl_{0.2}(OH)_{1.1}$ is mixed with Ce^{3+} and Ce^{4+} aqueous solution, respectively, the $Ce(OH)CO_3$ nanorod surface is clean in the former case (Fig. 5e) while plenty of "free" NPs are observed in the latter case (Fig. 5f), because the solubility product constant of $Ce(OH)_4$ is far smaller than that of $Ce(OH)_3$.

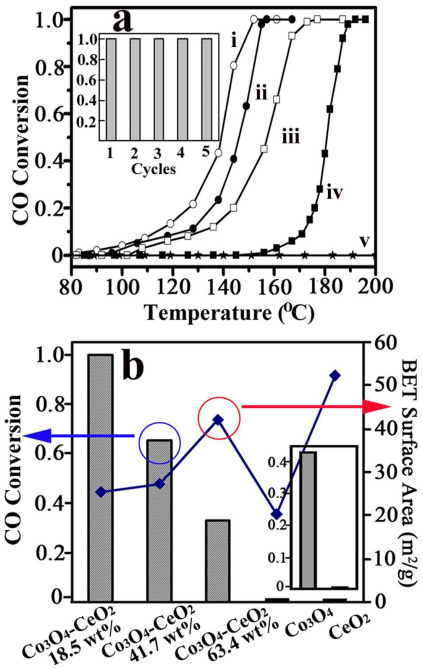

Fig. 6 (a) CO conversion as a function of temperature for Co_3O_4-CeO_2 bimetal oxide catalysts with different CeO_2 compositions: 18.5 wt% (i) 41.7 wt% (ii) 63.4 wt% (iii), and pure Co_3O_4 (iv), CeO_2 (v). (b) The comparisons in catalytic activity and BET surface area for the tested samples in (a). Inset in (a) shows the stability of Co_3O_4-CeO_2-18.5 wt% sample for catalytic oxidation under the conditions of (a).

Herein, CO catalytic oxidation, being a model reaction, was carried out to evaluate the catalytic performance of the obtained Co_3O_4-CeO_2 core-shell materials. As for comparison, the catalytic activities of pure Co_3O_4 rods derived from the thermal decomposition of $Co(CO_3)_{0.35}Cl_{0.2}(OH)_{1.1}$ precursor, and pure CeO_2 prepared by precipitation method were also examined. Their light-off curves (CO conversion rate *vs.* temperature) for CO oxidation are presented. The temperature for 50% of CO conversion (T_{50}) is an important parameter to assess the activity of the catalyst. As shown in Fig. 6a, pure Co_3O_4 shows the T_{50} at ~ 180 °C, while for the Co_3O_4-CeO_2 core-shell samples with different Co/Ce ratios, they exhibit higher catalytic activity than that of either pure Co_3O_4 or pure CeO_2. Specifically, the one with lowest content of CeO_2, Co_3O_4-CeO_2-18.5 wt %, exhibits the superior catalytic activity with the T_{50} at ~139 °C among all samples compared. Instead, the enrichment of CeO_2 induces the decrease of the catalytic activity, reflected as the increase of T_{50} for samples of Co_3O_4-CeO_2-41.7 wt% (T_{50} = 146 °C) and Co_3O_4-CeO_2-63.4 wt% (T_{50} = 157 °C). The pure CeO_2 sample does not show observable activity even at 200 °C. To evaluate the durability of the as-prepared Co_3O_4-CeO_2 catalyst, the Co_3O_4-CeO_2-18.5 wt% sample was selected as a typical example for successive CO oxidation test under the same experimental conditions. As shown in the inset of Fig. 6a, after five cycles up to 150 °C, the as-prepared Co_3O_4-CeO_2 catalyst still maintained almost 100% conversion rate of CO. Generally, the catalytic performance is closely related to the surface area of the catalysts. However, BET surface area analysis testified that no clear correlation between surface area and catalytic activity in our case, as shown in Fig. 6b. The pure CeO_2 possesses the largest surface area while displays the lowest catalytic activity. Even for the Co_3O_4-CeO_2 samples prepared from same procedure, the catalytic activity is independent on the surface area. These observations strongly suggest that the formation of the Co_3O_4-CeO_2 bimetal oxide structure catalyst introduces distinctly different and significant synergistic effect in the catalytic CO oxidation.

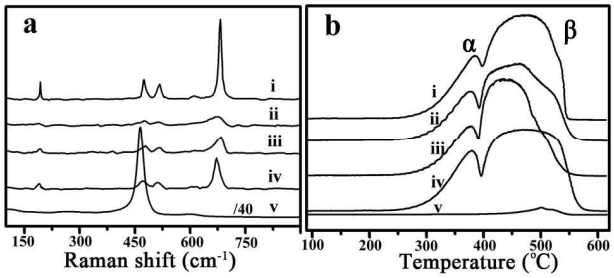

Fig. 7 Raman spectra (a) and H_2-TPR profiles (b) of pure Co_3O_4 (i), Co_3O_4-CeO_2-63.4 wt% (ii), Co_3O_4-CeO_2-41.7 wt% (iii), Co_3O_4-CeO_2-18.5 wt% (iv), and pure CeO_2(v).

It is widely recognized that the interaction between Co_3O_4 and CeO_2 is responsible for enhanced catalytic activity toward CO oxidation.[24,30] To investigate the surface chemistry feature of all samples, Raman spectroscopy characterization was performed. As illustrated in Fig. 7a of the Raman spectra, the band at ~466 cm^{-1} is related to the triply degenerated F_{2g} mode of fluorite CeO_2, and the bands at ~192, ~475, ~515, ~614 and ~682 cm^{-1} can be assigned to the vibrations of spinel Co_3O_4.[35] Interestingly, the peak intensity is strong at ~466 cm^{-1} for pure CeO_2, while nearly no obvious active Raman band can be detected at this position for all Co_3O_4-CeO_2 catalysts, indicating that the Co_3O_4 highly likely enables the closely contacted CeO_2 NPs to be structurally deformed.[36,37] H_2-TPR analysis was also conducted to study the interaction between Co_3O_4 and CeO_2. As shown in Fig. 7b, pure Co_3O_4 exhibits two reduction peaks (indexed as α, β), corresponding to the reductions of Co_3O_4 to CoO and CoO to metallic Co, respectively. In the case of Co_3O_4-CeO_2 catalysts, their reduction peaks (α) slightly shift to lower temperature in comparison to the pure Co_3O_4, further demonstrating a synergistic effect between Co_3O_4 and CeO_2.[30]

During CO catalytic oxidation, it is consensus that the whole process mainly involves the adsorption and desorption of gas molecules on the surface/or at the interface of the catalyst. In the case of Co_3O_4-CeO_2 structures, the synergistic interaction between Co_3O_4 and CeO_2 could modify Ce^{3+}/Ce^{4+} and Co^{2+}/Co^{3+} redox cycles and increases oxygen mobility. In addition, the oxygen vacancies, widely existed in CeO_2, could increase the adsorption amount and capacity of Co_3O_4-CeO_2 for oxygen molecules, and promote the dissociation of O_2 into O_{ads}, thus facilitating the CO oxidation. However, when the CeO_2 species increases to certain extent, *e.g.* Co_3O_4-CeO_2-63.4 wt% catalyst, it may significantly cover the Co_3O_4 surface, thus blocking the pore channel and causing the decrease of catalytic activity.[28,38]

4. Conclusions

In summary, Co_3O_4-CeO_2 core-shell catalysts were successfully synthesized by a facilely interfacial reaction between $Co(CO_3)_{0.35}Cl_{0.2}(OH)_{1.1}$ nanorods and Ce^{3+} aqueous solution, followed by a calcination step. The OH^- ions dissociated from $Co(CO_3)_{0.35}Cl_{0.2}(OH)_{1.1}$ combine with Ce^{3+} to form $Ce(OH)_3$, which can be easily convert into CeO_2 upon a calcination process. The small solubility product constant of $Ce(OH)_3$ is responsible for the heterogeneous nucleation of CeO_2 NPs onto the Co precursor surface, even in the absence of any surfactants or polymers. Moreover, the coverage degree of CeO_2 onto the Co_3O_4 rod surface can be tuned by changing the concentration of Ce^{3+} aqueous solution. The as-prepared Co_3O_4-CeO_2 core-shell catalysts display higher catalytic activity toward CO oxidation in comparison to either pure CeO_2 or Co_3O_4, indicating a strong synergistic effect between two components. This work also demonstrates the feasibility of designing core-shell structure by virtue of the utilization of solubility product constant difference, and also expands the strategies of preparing binary oxide catalysts by means of interfacial reactions.

Acknowledgements

This work is supported by the Shandong Provincial Natural Science Foundation, China (Grant no. ZR2015BM008), Scientific Research Foundation for the Returned Overseas Chinese Scholars, State Education Ministry.

Notes and references

1 E. W. Zhao, H. Zheng, R. Zhou, H. E. Hagelin-Weaver and C. R. Bowers, *Angew. Chem. Int. Ed.*, 2015, **54**, 14270-14275.
2 X. Liu, K. Zhou, L. Wang, B. Wang and Y. Li, *J. Am. Chem. Soc.*, 2009, **131**, 3140-3141.
3 J. Qi, J. Chen, G. Li, S. Li, Y. Gao and Z. Tang, *Energy Environ. Sci.*, 2012, **5**, 8937-8941.
4 M. Cargnello, N. L. Wieder, T. Montini, R. J. Gorte and P. Fornasiero, *J. Am. Chem. Soc.*, 2010, **132**, 1402-1409.
5 N. Ta, J. Liu, S. Chenna, P. A. Crozier, Y. Li, A. Chen and W. Shen, *J. Am. Chem. Soc.*, 2012, **134**, 20585-20588.
6 J. Ke, W. Zhu, Y. Jiang, R. Si, Y.-J. Wang, S.-C. Li, C. Jin, H. Liu, W.-G. Song, C.-H. Yan and Y.-W. Zhang, *ACS Catal.*, 2015, **5**, 5164-5173.
7 J. Ke, J.-W. Xiao, W. Zhu, H.-C. Liu, R. Si, Y.-W. Zhang and C.-H. Yan, *J. Am. Chem. Soc.*, 2013, **135**, 15191-15200.
8 A. Corma, T. Ródenasa and M. J. Sabater, *Chem. Sci.*, 2012, **3**, 398-404.
9 S. Song, X. Wang and H. Zhang, *NPG Asia Materials*, 2015, **7**, 179-197.
10 W. Shi, Y. Li, J. Hou, H. Lv, X. Zhao, P. Fang, F. Zheng and S. Wang, *J. Mater. Chem. A,* 2013, **1**, 728-734.
11 Q. Shen, M. Wu, H. Wang, C. He, Z. Hao, W.Wei and Y. Sun, *Catal. Sci. Technol.,* 2015, **5**, 1941-1952.
12 Y. Zhang, Y. Yu and H. He, *Catal. Sci. Technol.,* 2016, **6**, 3950-3962.
13 A. V. Porsin, E. A. Alikin and V. I. Bukhtiyarov, *Catal. Sci. Technol.*, 2016, Advance Article.
14 C. Tang, H. Zhang and L. Dong, *Catal. Sci. Technol.,* 2016, **6**, 1248-1264.
15 X. Guo and R. Zhou, *Catal. Sci. Technol.,* 2016, **6**, 3862-3871.
16 B. Liu, Y. Liu, H. Hou, Y. Liu, Q. Wang and J. Zhang, *Catal. Sci. Technol.,* 2015, **5**, 5139-5152.
17 S. Sun, D. Mao, J. Yu, Z. Yang, G. Lu and Z. Ma, *Catal. Sci. Technol.,* 2015, **5**, 3166-3181.
18 B. Liu, Y. Liu, C. Li, W. Hua, P. Jing, Q. Wang and J. Zhang, *Applied Catalysis B: Environmental*, 2012, **127**, 47-58.
19 Q. Wang, Y. Li, B. Liu, Q. Dong, G. Xu, L. Zhang and J. Zhang, *J. Mater. Chem. A*, 2015, **3**, 139-147.
20 H. Bao, Z. Zhang, Q. Hua and W. Huang, *Langmuir*, 2014, **30**, 6427-6436.
21 N. S. Arul, D. Mangalaraj, R. Ramachandran, A. N. Grace and J. I. Han, *J. Mater. Chem. A*, 2015, **3,** 15248-15258.
22 X. Wang, S. Zhao, Y. Zhang, Z. Wang, J. Feng, S. Song and H. Zhang, *Chem. Sci.*, 2016, **7**, 1109-1114.
23 M. Zabilskiy, P. Djinović, E. Tchernychova, O. P. Tkachenko, L. M. Kustov and A. Pintar, *ACS Catal.*, 2015, **5**, 5357-5365.
24 J. Zhen, X. Wang, D. Liu, S. Song, Z. Wang, Y. Wang, J. Li, F. Wang and H. Zhang, *Chem. Eur. J.*, 2014, **20**, 4469-4473.
25 J. Cui, X. Zhang, L. Tong, J. Luo, Y. Wang, Y. Zhang, K. Xie and Y. Wu, *J. Mater. Chem. A*, 2015, **3**, 10425-10431.
26 P. Sudarsanam, B. Hillary, B. Mallesham, B. G. Rao, M. H. Amin, A. Nafady, A. M. Alsalme, B. M. Reddy and S. K. Bhargava, *Langmuir*, 2016, **32**, 2208-2215.
27 J. Qin, J. Lu, M. Cao and C. Hu, *Nanoscale.*, 2010, **2**, 2739-2743.
28 J. Shi, *Chem. Rev.*, 2013, **113**, 2139-2181.
29 J. Yang, L. Lukashuk, J. Akbarzadeh, M. Stöger-Pollach, H. Peterlik, K. Föttinger, G. Rupprechter and U. Schubert, *Chem. Eur. J.,* 2015, **21**, 885-892.
30 J. Zhen, X. Wang, D. Liu, Z. Wang, J. Li, F. Wang, Y. Wang and H. Zhang, *Nano Res.*, 2015, **8**, 1944-1955.
31 M. B. Gawande, A. Goswami, T. Asefa, H. Guo, A. V. Biradar, D.-L. Peng, R. Zboril and R. S. Varma, *Chem. Soc. Rev.*, 2015, **44**, 7540-7590.
32 G. Chen, F. Rosei and D. Ma, *Adv. Funct. Mater.*, 2012, **22**, 3914-3920.
33 S. Sun and Z. Yang, *Chem. Commun.*, 2014, **50**, 7403-7415.
34 M. Sytnyk, R. Kirchschlager, M. I. Bodnarchuk, D. Primetzhofer, D. Kriegner, H. Enser, J. Stangl, P. Bauer, Mi. Voith, A. W. Hassel, F. Krumeich, F. Ludwig, A. Meingast, G. Kothleitner, M. V. Kovalenko and W. Heiss, *Nano Lett.*, 2013, **13**, 586-593.
35 H. Wang, D. Ma, X. Huang, Y. Huang, X. Zhang, *Sci. Rep.*, 2012, **7**, 701.
36 B. M. Reddy, A. Khan, Y. Yamada, T. Kobayashi, S. Loridant and J. C. Volta, *J. Phys. Chem. B*, 2003, **107**, 11475-11484.
37 J. Liu, Z. Zhao, J. Wang, C. Xu, A. Duan, G. Jiang and Q. Yang, *Applied Catalysis B: Environmental*, 2008, **84**, 185-195.
38 G. Chen, Q. Xu, Y. Yang, C. Li, T. Huang, G. Sun, S. Zhang, D. Ma and X. Li, *ACS Appl. Mater. Interfaces*, 2015, **7**, 23538-23544.

Graphical Abstract

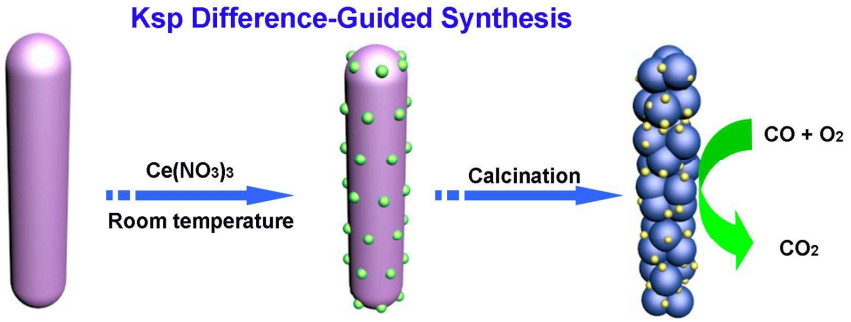

Ion exchange procedure, one kind of solid-liquid interfacial reactions, is so far restricted to chalcogenide based core-shell nanomaterials, in contrast, the bimetal oxide with core-shell structures by means of ion exchange has not extensively studied yet. Herein, Co_3O_4-CeO_2 core-shell catalysts are successfully fabricated by an ion exchange procedure between $Co(CO_3)_{0.35}Cl_{0.2}(OH)_{1.1}$ nanorods and Ce^{3+} aqueous solution, followed by a calcination step.